Deformable Boundary EIT for Breast Cancer Imaging

Jing Hu, Manuchehr Soleimani

Engineering Tomography Lab (ETL), Department of Electronic and Electrical Engineering, University of Bath, Bath, UK:

jh460@bath.ac.uk, m.soleimani@bath.ac.uk

Abstract: Electrical impedance tomography (EIT) has been investigated as a potential non-invasive method for breast cancer imaging for more than two decades. However, since EIT requires direct contact with the boundary, electrode positioning and boundary movement have always been considered as two of the sources of errors and artifacts. A breast can be deformed due to its natural structure. Therefore, if the breast is deformed on purpose, each deformation can provide one new set of independent EIT measurements data. More independent data provides more information from the same region of interest. In this hypothesis, information gathered with different deformations is combined, in all cases we assumed that shape and electrode positions measured by other means. Simulations have been carried out to verify the hypothesis, and results show improvements in the detectability of the early stage tumor in depth.

Keywords: Electrical impedance tomography, breast cancer imaging, deformable boundary

1. Introduction

Breast Cancer is one of the most common cancers in women; only in the England 46085 women and 332 men were diagnosed with invasive breast cancer in 2014 (Office for National Statistics, 2016).There are various stages of breast cancer based on the size of the tumour, lymph node invasion and whether metastatic spread (the TNM system) (Taherian-Fard, Srihari, & Ragan, 2014). The curative ratio and survival rate are much higher at early stages with smaller tumours. The mortality rate decreased by 34% from 1990-2010 in the US (Nagwa Dongola, 2015). Screening methods, such as mammography, have been one of the biggest contributors to the reduction of the mortality rate. Early detection of the tumours in their primary stage will substantially increase the patient's chance of living. Mammography has been used as the standard screening and diagnosis tool for breast cancer. However, a study shows that it can also cause unnecessary pain and can lead to surgeries due to false diagnoses and over-diagnoses (Mulcanhy, 2015). In relatively rare cases (less than 1%) defined as ‘occult’ breast cancer, patients presenting metastasized

carcinoma to the axillary lymph node without mammographic or physical finding of the primary (Lloyd & Nash, 2001). Also, since it is X-ray sourced, mammography is considered to be invasive.

Electrical Impedance Tomography (EIT) is an imaging technique under investigation as an alternative imaging method for breast cancer screening. Studies (SHA, WARD, & STORY, 2002) have shown that normal breast tissue and benign tumours have similar conductivity properties, but there is a big contrast between normal/benign and malignant breast tissue at low frequency (1 kHz-1MHz). These studies indicate that electrical conductivity properties can be used to identify breast cancer. The principle of EIT is to reconstruct the image of the region of interest by mapping the conductivity distribution of the area with the measurements taken at the boundary. Among all the medical imaging technologies, EIT has the advantages of being low cost, mobile and non-invasive.

However, since EIT requires direct contact with the boundary (in this case the skin), electrodes positioning errors and boundary movement have been considered as one of the sources of errors. Previous studies (Boyle, Adler, & Lionheart, 2012) worked on shape recovery and correction to reduce the errors. However, unlike other parts of body such as the brain and the thorax, breast tissues are more elastic, and thus the deformation of the boundary shape is achievable. The scheme of turning the issue into an opportunity for breast cancer application of EIT is investigated in this paper. In this scheme, with the deformation of the boundary shape of the breast, increasing numbers of independent measurements can be collected without physically moving the electrodes that are attached to the human body. Multiple independent measurements can provide more information about the region of interest. Theoretically, combining these additional pieces of information would increase the detectability of smaller tumours. Computational simulations have been carried out to verify this hypothesis. Conclusions are drawn from the simulation results using total variation (TV) regularisation as well as more commonly used Tikhonov regularisation scheme.

2. Methods

2.1)Forward modelling

EIT systems consist of electrodes on the boundary for driving and measuring purposes. For the appropriate formulation of the system, the complete electrode model (CEM) was introduced in 1999 (Vauhkonen, Vauhkonen, Savolainen, & Kaipio, 1999) to constrain the boundary conditions. Equation

$$\boldsymbol{\nabla \cdot (\sigma \nabla u) = 0 \;\; x \in \Omega} \quad (1)$$

describes the potential field within the boundary, and the voltage measurement at the electrode U_k is described by the complete electrode model

$$\mathbf{U_k} = \mathbf{u} + \mathbf{Z_k}\boldsymbol{\sigma}\frac{\partial \mathbf{u}}{\partial \hat{\mathbf{n}}} \quad \mathbf{x} \in \mathbf{e_k}\,; \mathbf{k} = \mathbf{1}, \mathbf{2}, \ldots, \mathbf{k} \qquad (2)$$

Where u is the potential field, Z_k is the contact impedance, $\hat{n}$ is the outward unit normal vector and e_k is the electrodes. The driving current I_k is described by the Dirichlet boundary condition, I_k can be seen as an integral of the inward current density on the electrode surface S

$$\mathbf{I_k} = \int_{\mathbf{e_k}} \hat{\boldsymbol{\sigma}}\, \frac{\partial \mathbf{u}}{\partial \hat{\mathbf{n}}}\, \mathbf{ds} \quad \mathbf{x} \in \mathbf{e_k} \quad \mathbf{k} = \mathbf{1}, \mathbf{2}, \ldots, \mathbf{k} \qquad (3)$$

The inter-electrode gaps on the boundary is described by

$$\hat{\boldsymbol{\sigma}}\frac{\partial \mathbf{u}}{\partial \hat{\mathbf{n}}} = \mathbf{0} \;\; \mathbf{x} \in \boldsymbol{\partial\Omega} \quad \text{but not on} \quad \mathbf{e_k} \qquad (4)$$

To ensure a unique solution for the system, more constraints are applied based on the law of charge conservation, and a reference point is selected.

$$\sum_{\boldsymbol{k=1}}^{\boldsymbol{k}} \boldsymbol{I_k} = \mathbf{0} \qquad (5)$$

$$\boldsymbol{V_r} = \mathbf{0} \qquad (6)$$

To be able to image a domain, it is essential to turn the continuous problem into a discrete problem. The finite element method (FEM) is a numerical discretizing method commonly used in EIT, and it discretizes the domain of interest into small elements to solve the forward model. Equations for FEM formulations and the Jacobian calculation are partially taken from (Lionheart, Polydorides, & Borsic, 2005).The potential distribution is approximated into finite elements using the linear piecewise function:

$$\boldsymbol{u_h}(\boldsymbol{x}) = \sum_{\boldsymbol{i=1}}^{\boldsymbol{N}} \boldsymbol{u_i}\boldsymbol{\phi_i}\,(\boldsymbol{x}) \qquad (7)$$

Where N is the number of nodes, ϕ_i is the nodal basis function and u_i is the nodal value assumed by the solution.

However, since ϕ_i are not differentiable, Equation (1) can't be satisfied and

$$\boldsymbol{\nabla} \cdot (\boldsymbol{\sigma}\boldsymbol{\nabla}\boldsymbol{u_h}) \neq \mathbf{0} = \boldsymbol{r} \qquad (8)$$

Where r is residual. Instead, we drive a weaker form of equation and according to the Galerkin Method/Weighted residuals method, with proper choice of the shape function ω

$$\int_{\boldsymbol{\Omega}} \boldsymbol{\omega}\boldsymbol{\nabla} \cdot (\boldsymbol{\sigma}\boldsymbol{\nabla}\boldsymbol{u_h})\boldsymbol{d\Omega} = \mathbf{0} \qquad (9)$$

Using Green's Second identity and the vector identity

$$\boldsymbol{\nabla \cdot (\omega \sigma \nabla u_h) = \sigma \nabla u_h \cdot \nabla \omega + \omega \nabla \cdot (\sigma \nabla u_h)} \quad (10)$$

Therefore with partial integral and divergence theorem

$$\boldsymbol{\int_{\Omega} \sigma \nabla u_h \cdot \nabla \omega \, d\Omega = \int_{\Gamma_1} \sigma \nabla u_h \cdot \hat{n} \, \omega dS + \int_{\Gamma_2} \sigma \nabla u_h \cdot \hat{n} \, \omega dS} \quad (11)$$

Where Γ_1 is the surface of the boundary with electrodes and Γ_2 is the inter-electrode parts (no electrodes). The current density between the electrodes are zero therefore

$$\boldsymbol{\int_{\Gamma_2} \sigma \nabla u_h \cdot \hat{n} \, \omega dS = 0} \quad (12)$$

With complete electrodes model,

$$\int_{\Omega} \sigma \nabla u_h \cdot \nabla \omega \, d\Omega = \int_{\Gamma_1} \frac{U_k - u_h}{Z_k} \omega dS \quad (13)$$

$$= \boldsymbol{\sum_{k=1}^{k} \int_{e_k} \frac{1}{z_k} (U_k - u_h) \omega dS \;\; x \in e_k \qquad k = 1, 2, \dots, k} \quad (14)$$

In FEM, the same test function is used for both the shape function and the potential approximation. I.e. $\omega = \sum_{j=1}^{N} \phi_j$ and $u_h = \sum_{i=1}^{N} u_i \phi_i$.

The FEM system equation is built in the format below

$$\begin{bmatrix} \boldsymbol{A_M + A_Z} & \boldsymbol{A_W} \\ \boldsymbol{A_W^T} & \boldsymbol{A_D} \end{bmatrix} \begin{bmatrix} \boldsymbol{u} \\ \boldsymbol{U} \end{bmatrix} = \begin{bmatrix} \boldsymbol{0} \\ \boldsymbol{I} \end{bmatrix} \quad (15)$$

Where A_M and A_Z are $n \times n$ matrices, A_W is $n \times k$ and A_D is $k \times k$ dimensions matrices. And

$$\boldsymbol{A_M(i,j) = \int_{\Omega} \nabla \phi_i \nabla \phi_j d\Omega}$$

$$\boldsymbol{A_Z(i,j) = \sum_{k=1}^{k} \int_{e_k} \frac{1}{Z_k} \phi_i \phi_j dS}$$

$$\boldsymbol{A_W(i,j) = -\frac{1}{Z_k} \int_{e_k} \phi_i \, dS}$$

$$\boldsymbol{A_D = diag\left(\frac{E_k}{Z_k}\right)}$$

The Jacobian matrix is "the complete matrix of partial derivatives of voltages with respect to conductivity parameters" (Lionheart, Polydorides, & Borsic, 2005). The current input is kept constant, and the perturbations are:$\sigma \to \sigma + \delta\sigma$,$u \to u + \delta u$ and $U_k \to U_k + \delta U_k$ .Then the first order perturbation is calculated, and the total change in power is

$$\sum_k \bar{I}_k \delta U_k = \int_\Omega \delta\sigma |\nabla u|^2 d\Omega \qquad (16)$$

To get the potential change on a particular electrode e_m ,the current pattern is considered and solved: $\bar{I}_k^m = \delta_{km}$. $u(I^m)$ is the hypothetical measurement potential and the current for dth driving pattern is $u(I^d)$.

$$\delta U_{dm} = -\int_\Omega \delta\sigma \nabla u(I^d) \cdot \nabla u(I^m) d\Omega \qquad (17)$$

To calculate the Jacobian matrix one must choose a discretization of the conductivity. The simplest case is to take the conductivity to be the piecewise constant on polyhedral domains such as voxels or tetrahedral elements. Taking $\delta\sigma$ to be the characteristic function of the kth voxel $\Omega_k$we have for a fixed current pattern

$$J_{dmk} = \frac{\delta U_{dm}}{\delta \sigma_k} = -\int_{\Omega_k} \nabla u(I^d) \cdot \nabla u(I^m) d\Omega \qquad (18)$$

2.2) Combination of deformed boundary shapes

In our case, one of the major challenges is that with deformable boundary, the boundary shapes change for each set of measurements. Therefore, with multiple shapes, multiple forward models are required. At this stage, the selection of shapes is entirely arbitrary. Six different meshes for each particular shape are generated for the first step simulation（Figure 1）. All of the meshes are 2D, and 16 electrodes are placed around the boundary. The x-dimension of all meshes are kept as 1.The limitations of deformation and the choice of shapes will be investigated in the future. Ideally, in the final application combined with the experimental data, the program should be able to gather the actual shape deformation of the phantom and generate meshes accordingly. To combine these different sets of information, a square of the region of interest is selected with the inclusion inside. To maintain the consistency of the Jacobian matrix, the inclusion within the region will not change with the deformation. Also, a 30 x 30 grid mesh is used instead of a triangular mesh. To combine the information, a super Jacobian matrix is formed and the equation of the system is as follows:

$$\begin{bmatrix} \Delta \mathbf{V_1} \\ \Delta \mathbf{V_2} \\ \vdots \\ \Delta \mathbf{V_6} \end{bmatrix} = [\mathbf{J_1}; \mathbf{J_2}; \cdots; \mathbf{J_6}](\Delta \mathbf{x}) \qquad (19)$$

Where $\Delta V_1, \Delta V_2, \Delta V_3, \Delta V_4, \Delta V_5, \Delta V_6$ are the voltage difference data for shape 1, 2, 3, 4, 5 and 6, and $\mathbf{J_1}, \mathbf{J_2}, \mathbf{J_3}, \mathbf{J_4}, \mathbf{J_5}, \mathbf{J_6}$,are the Jacobian values for each shape.

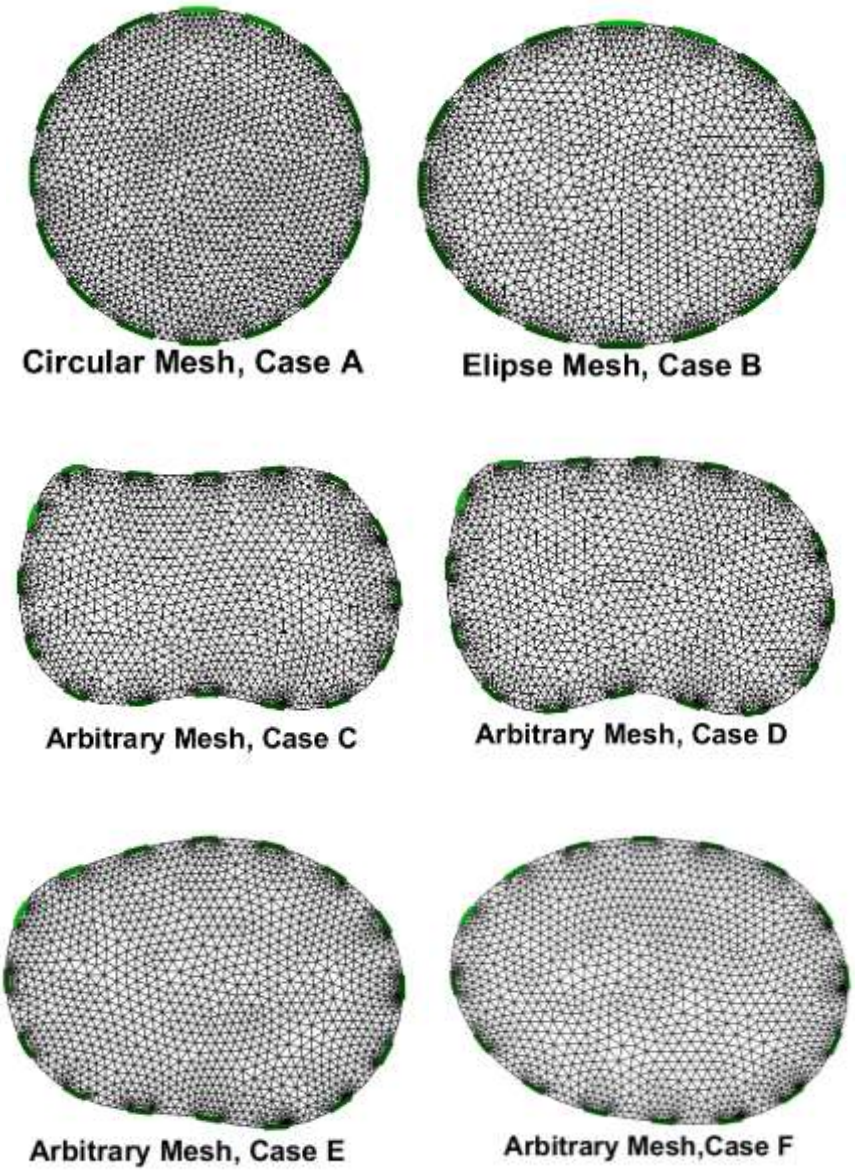

Figure 1 Six different meshes that are generated for six different shapes

2.2) Information content in combined data

Singular Value Decomposition (SVD) is a decomposition method used to transform a set of high-dimensional correlated data into a set of lower dimensional uncorrelated data that expose the desired relationship more clearly than the original data set. The dimensions are identified and ordered from most to least variation. With SVD, we can greatly reduce the amount of data by cutting off variables below a certain threshold. However, the main relationship in which we are interested is maintained.

A $m \times n$ rectangular or square matrix A can be decomposed into three matrices:

$$\boldsymbol{A_{m\times n} = U_{m\times m} S_{m\times n} V^T_{n\times n}} \qquad (\mathbf{20})$$

Where U is an m × m orthonormal matrix, and the columns of U are the orthonormal eigenvectors of AA^T. S is a m × n diagonal matrix and it contains the square root of non-zero eigenvalues from U or V in descending order (eigenvalues from U and V are always the same).V is an n × n orthonormal matrix and the columns of V is the orthonormal eigenvectors of $A^T A$. And $V^T$is the transpose of matrix V, and it is a n × n matrix.

The columns of U are called left singular vectors and the columns of V are called right singular vectors. The diagonal entries in matrix S constitute the singular value of matrix A. This indicates the variance of the independent components along each dimension.

Assume that u_1, v_1 and σ_i are numbers and order that $\sigma_1 \geq \sigma_2 \geq \cdots \geq \sigma_r > 0 = \sigma_{r+1} = \cdots = \sigma_n$ the expression of matrix A can be then written as:

$$\boldsymbol{A = (u_1 \cdots u_r)\begin{pmatrix} \sigma_1 & & \\ & \ddots & \\ & & \sigma_r \end{pmatrix}\begin{pmatrix} V_1^T \\ \vdots \\ V_r^T \end{pmatrix}} \qquad (\mathbf{21})$$

If $\sigma_{t+1}, \ldots, \sigma_r$ are negligibly small, matrix A can be approximated and SVD can be truncated into many fewer dimensions:

$$\boldsymbol{A \approx (u_1 \cdots u_t)\begin{pmatrix} \sigma_1 & & \\ & \ddots & \\ & & \sigma_t \end{pmatrix}\begin{pmatrix} V_1^T \\ \vdots \\ V_t^T \end{pmatrix}} \qquad (\mathbf{22})$$

This reduction will not affect the main relationship of the data, since the components are ordered from most to least variation. Cutting off less significant elements can also exclude noises very effectively.

Figure 2 is the SVD decay for different cases and also for the combined Jacobian. The graph in Figure 2 shows the potential improvements this scheme might bring. Above a given noise level, the number of independent measurements increases significantly with the combination of the Jacobian.

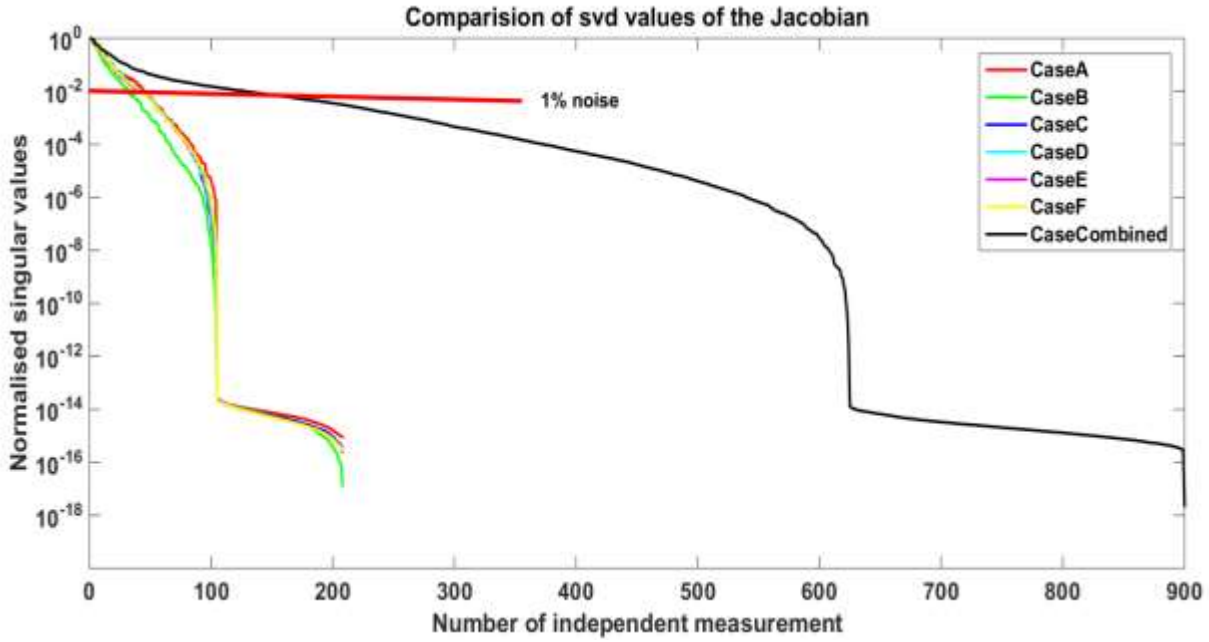

Figure 2 SVD of the Jacobian matrix of six individual shapes and combined data

2.3) Tikhonov and TV reconstruction methods

We have implemented both the standard Tikhonov regularization method and the Bregman TV methods (Goldsteom & Osher, 2009) for image reconstruction. The Standard Tikhonov method can be used to calculate the change in conductivity

$$\Delta \mathbf{x} = (\mathbf{J^T J} + \boldsymbol{\gamma}^2 \mathbf{I})^{-1} \mathbf{J^T} \Delta \mathbf{v} \qquad (23)$$

The total variation problem is defined by adding a penalty term the $l_1 - norm$ of the gradient of the image, or the so called total variation regularization term $G_{TV}\ (\Delta x)$

$$\boldsymbol{G_{TV}}\ (\Delta \boldsymbol{x}) = \boldsymbol{\alpha R}(\Delta \boldsymbol{x}) = \boldsymbol{\alpha} \|\boldsymbol{\nabla}\, \Delta \boldsymbol{x}\|_{\mathbf{1}} \qquad (24)$$

Where α is the regularization parameter based on the Bregman iterative algorithm, split Bregman methods (Goldsteom & Osher, 2009) can extend the utility of the Bregman iteration to the minimizations of more general $l_1 - norm$ regularization terms. The same algorithms are applied both to the combined data case and the individual cases such as case A (circular shape). TV functional can be described in domain **Ω**:

$$\boldsymbol{Reg}(\Delta \boldsymbol{x})^{\boldsymbol{TV}} = \int_{\boldsymbol{\Omega}} |\boldsymbol{\nabla}(\Delta \boldsymbol{x})| \, \boldsymbol{d\Omega} \tag{25}$$

Then the Bregman iterative algorithm can be expressed as following

$$\Delta \boldsymbol{x}^{\boldsymbol{k+1}} = \mathbf{Min}\, \boldsymbol{D}_{\boldsymbol{R}} \left(\Delta \boldsymbol{x}, \Delta \boldsymbol{x}^{\boldsymbol{k}}\right) + \frac{\boldsymbol{\lambda}}{\mathbf{2}} \|\boldsymbol{J}\Delta \boldsymbol{x} - \Delta \boldsymbol{v}\|^{\mathbf{2}} \tag{27}$$

The sub gradient of the total variation function at the $(k+1)\ th$-iteration

$$s^{k+1} = s^{k} - \lambda J^{T}(J\Delta x^{k+1} - \Delta \boldsymbol{v}) \tag{28}$$

Equation ((27) and (28) are the basic formulation split Bregman TV method

$$\Delta x^{k+1} = \boldsymbol{argmin}\{\, R\,(\Delta x) + \frac{\lambda}{2} \left\| J\Delta x - (\Delta \boldsymbol{v})^{k} \right\|^{2} \} \tag{29}$$

$$(\Delta \boldsymbol{v})^{k+1} = (\Delta \boldsymbol{v})^{k} + \Delta \boldsymbol{v} - J\Delta x^{k+1} \tag{30}$$

The split Bregman iteration method is introduced as follows: an auxiliary variable d which aims to be optimised to represent $(d = \Delta x)$ can be used to allow solving a constrained optimization problem

$$\boldsymbol{x}_{\boldsymbol{\alpha}} = \boldsymbol{argmin}_{\Delta x} \frac{\mathbf{1}}{\mathbf{2}} \|\boldsymbol{J}\Delta \boldsymbol{x} - \Delta \boldsymbol{v}\|^{\mathbf{2}} + \boldsymbol{\alpha}\|\boldsymbol{d}\|_{\mathbf{1}} \tag{31}$$

To solve this problem, the corresponding unconstrained optimization problem of equation (31) is

$$x_{\alpha} = argmin_{\Delta x} \frac{1}{2} \|J\Delta x - \Delta \boldsymbol{v}\|^{2} + \alpha \|d\|_{1} + \frac{\beta}{2} \|d - \Delta x\|^{2} \tag{32}$$

Where $\beta > 0$ is the split parameter. After applying the Bregman iteration method that shown in equation (29) and (30), the solution of equation (32) can be obtained as following

$$(\Delta x^{k+1}, d^{k+1}) = argmin_{\Delta x, d} \frac{1}{2} \|J\Delta x - \Delta \boldsymbol{v}\|^{2} + \alpha \|d\|_{1} + \frac{\beta}{2} \left\| d - \Delta x - b_{d}^{k} \right\|^{2} \tag{33}$$

$$b_{d}^{k+1} = b_{d}^{k} + \Delta x^{k+1} - d^{k+1} \tag{34}$$

2.4) Experimental Setup

To be consistent with the simulation study, six phantoms scaled from the simulation had been 3D-printed. Electrodes are attached corresponding to the computer model. The electrode positioning used in 3D EIT for brain activity (Tidswell, Gibson, Bayford, & Holder, 2000) may be applied to breast cancer in future work. Location of inclusions for all sets of experiments are marked with same scale. Figure 3 is a picture of the printed phantoms we used for tests.

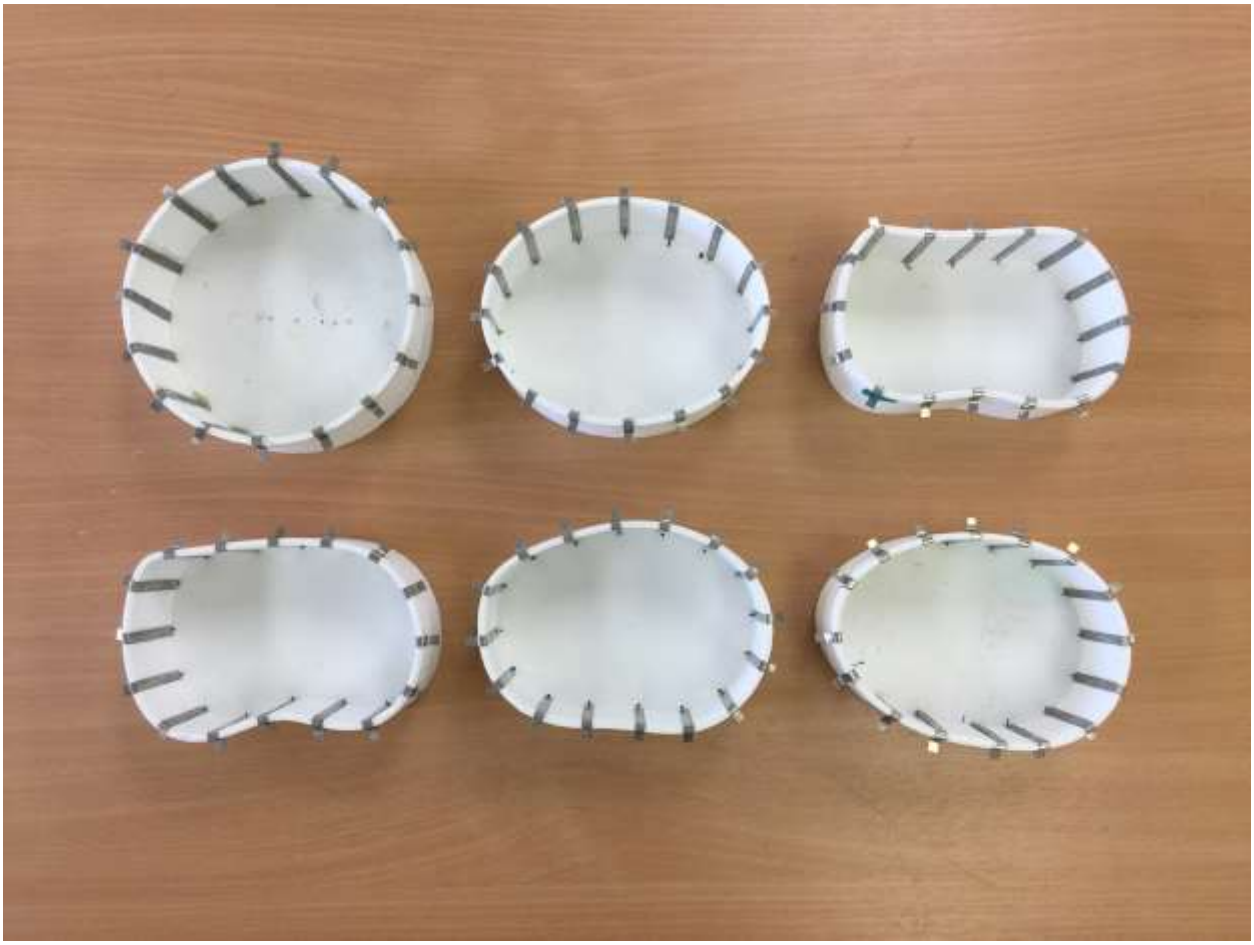

Figure 3 Picture of 3D printed phantom

KHU Mark 2.5 multi-frequency EIT system is used for the experiments. This is developed by Impedance Imaging Research Centre and Department of Biomedical Engineering of Kyung Hee University in South Korea. (Oh, Wi, Kim, Yoo, & Woo, 2011). Figure 4 is a picture of connected system.

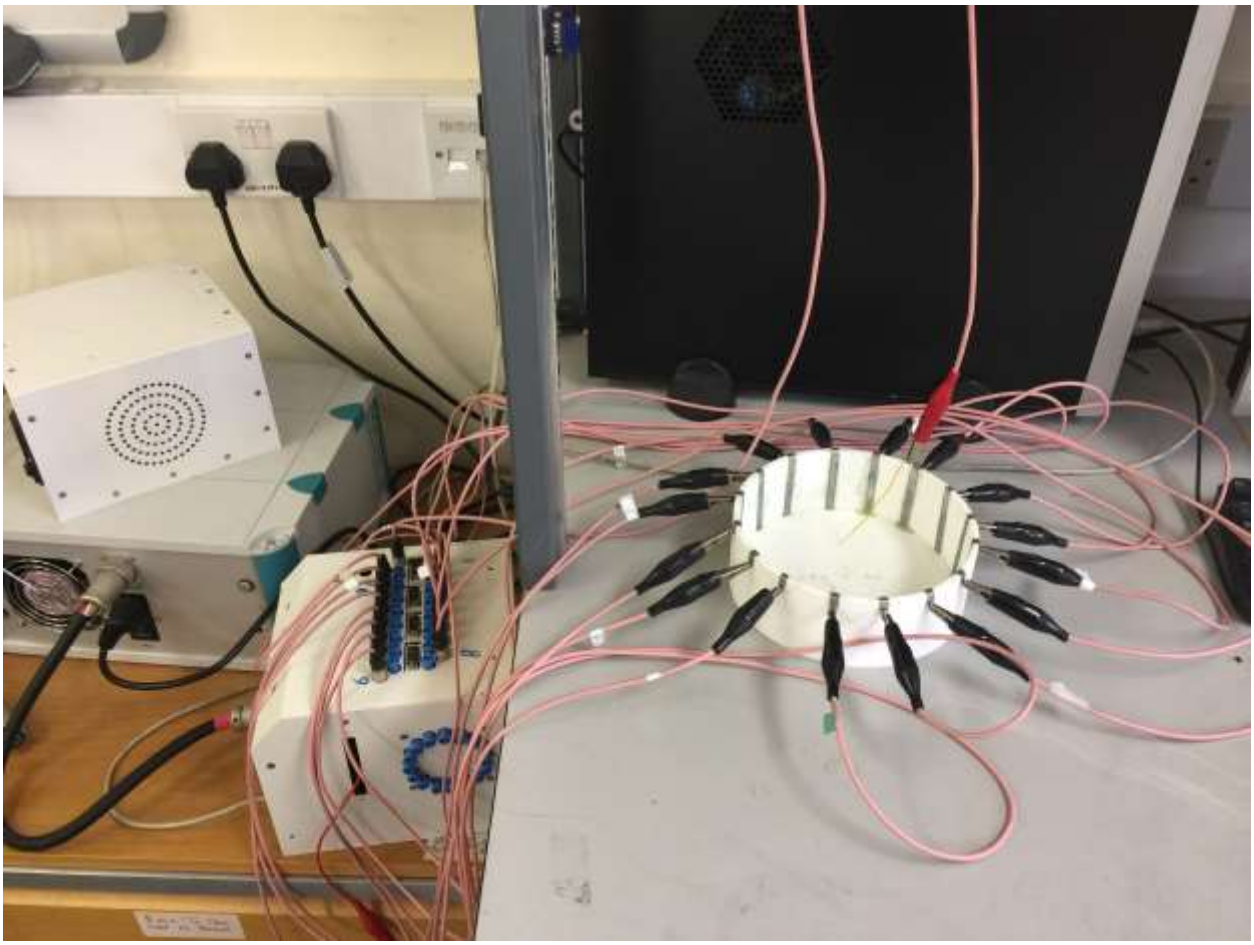

Figure 4 Picture of connected system

Some initial tests had been carried out to verify the feasibility of physical experimentation. Table 1 below shows reconstructions for some of the individual deformed shapes.

Table 1 Reconstructions for individual shapes

	Picture of actual positions	Reconstruction with phantom data
Case C	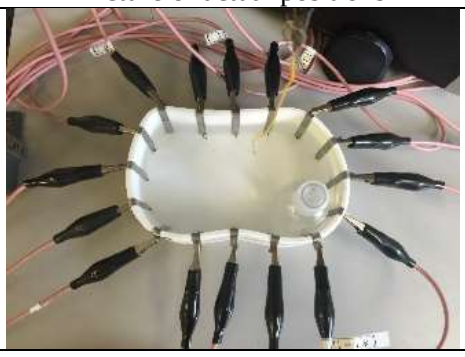	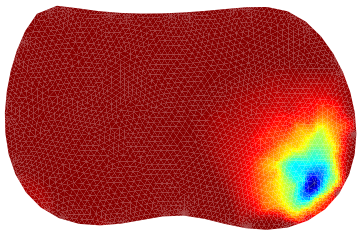

	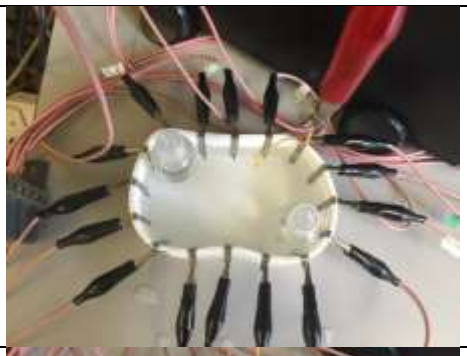	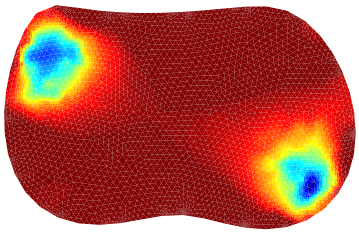
Case E		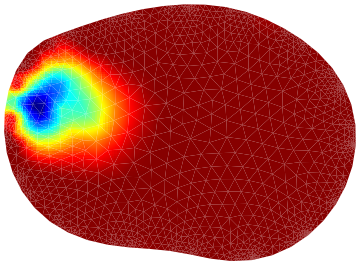
		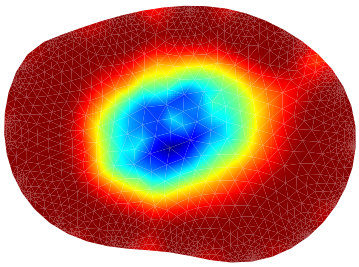
Case F	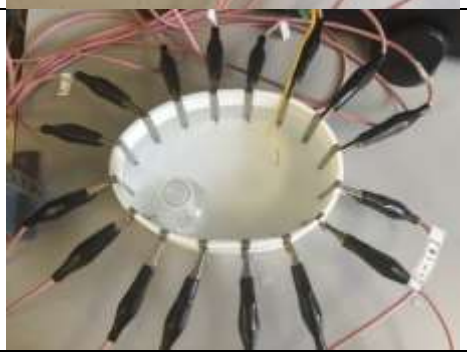	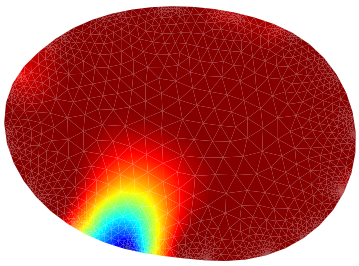

3. Simulation Results

To evaluate the performance of combined data, a number of simulation studies are being carried out. In all cases the electrical conductivity of background is 1 S/m and inclusions has electrical conductivity of 1.1

S/m. For each set of simulations, 2% Gaussian noise (2% of the mean value of the measured voltage differences) is added to all simulations. Each table shows ROI, inclusion, and reconstruction using the TV and the Tikhonov methods for both Case A (circular shape) and for combined data sets. For example, in Table 2, Set 1 simulates an inclusion of size 0.2 located at the centre of the region (0, 0). A true image of the inclusion with the circular shape (Case A) is shown on the top right. A reconstruction comparison between the circular case (Case A) and the combined case with both Tikhonov regularization and total variation is shown for each set.

The first nine sets of simulations are with single inclusions to study the effect of size and location on image reconstruction. Results show a much-improved performance of the combined data set with a small tumour model. Table 6 and

Table 9 indicate that for both Tikhonov and TV, the combined methods produce a better image than Case A. When 2% noise data is added and the model is run multiple times, the combined case shows consistent results, while Case A will be affected by high level of artefacts.

Table 9 shows a simulation with a small inclusion in the centre that the single data set has completely failed to detect the inclusion. In comparison, the combined case shows a circular inclusion with correct position. This show potential of proposed combined method for early detection of breast cancer.

Table 2 :Set1 simulation with single inclusion of radius 0.2 at location (0, 0)

<table>
<tr><td></td><td>Location</td><td>Size</td><td colspan="2"></td></tr>
<tr><td>SET 1</td><td>(0,0)</td><td>r =0.2</td><td colspan="2">True Image of the inclusion with circular shape(Case A)</td></tr>
<tr><td rowspan="4"></td><td rowspan="4"></td><td rowspan="4"></td><td colspan="2"> 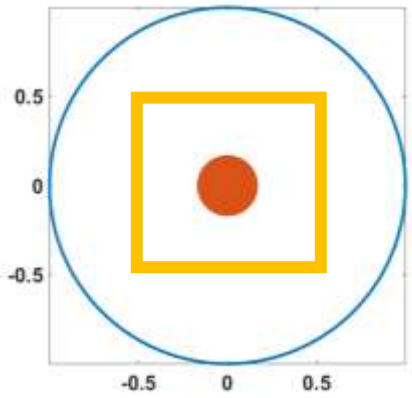
</td></tr>
<tr><td>CaseA(Tikhonov with 2% noise)</td><td>CaseA(TV with 2% noise)</td></tr>
<tr><td> 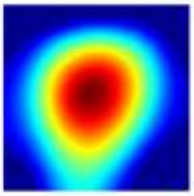 </td><td> 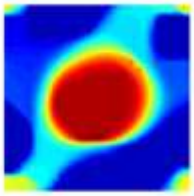 </td></tr>
<tr><td>Combined(Tikhonov with 2%noise)</td><td>Combined(TV with 2%noise)</td></tr>
</table>

			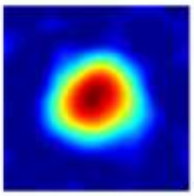	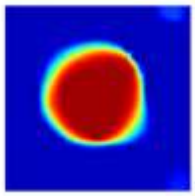

Table 3: Set 2 Simulation with Single Inclusion of Radius 0.2 at Location (0.2, 0)

	Location	Size		
SET 2	(0.2,0)	r =0.2	True Image of the inclusion with circular shape(Case A)	
			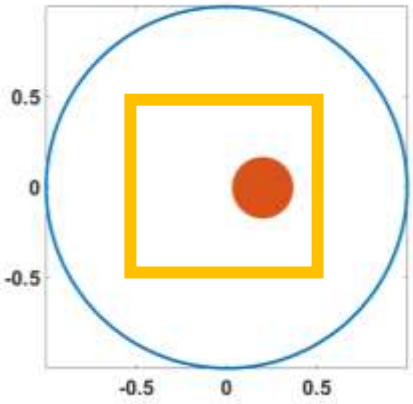	
			CaseA(Tikhonov with 2% noise)	CaseA(TVwith 2% noise)
			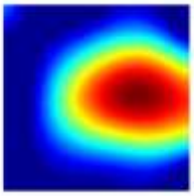	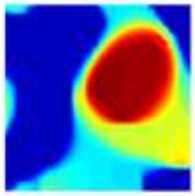
			Combined(Tikhonov with 2%noise)	Combined(TV with 2%noise)

			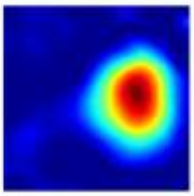	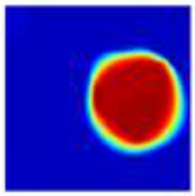

Table 4: Set3 Simulation with Single Inclusion of Radius 0.2 at Location (0.1, 0)

	Location	Size		
SET 3	(0.1,0)	r =0.2	True Image of the inclusion with circular shape(Case A)	
			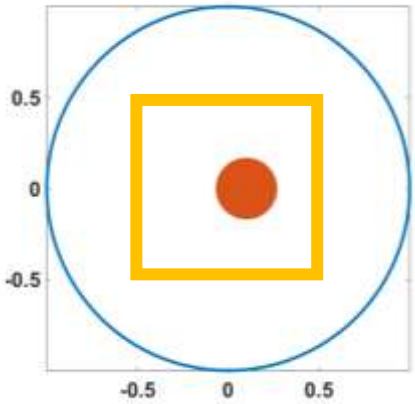	
			CaseA(Tikhonov with 2% noise)	CaseA(TV with 2% noise)
			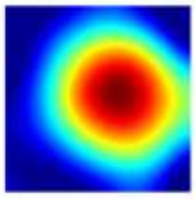	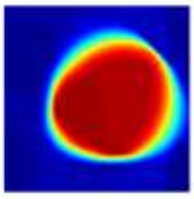
			Combined(Tikhonov with 2%noise)	Combined(TV with 2%noise)

			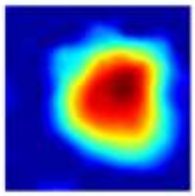	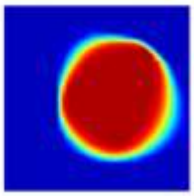

Table 5 :Set4 Simulation with Single Inclusion of Radius 0.2 at Location (-0.2, 0)

<table>
<tr><td></td><td>Location</td><td>Size</td><td colspan="2"></td></tr>
<tr><td rowspan="6">SET 4</td><td rowspan="6">(-0.2,0)</td><td rowspan="6">r =0.2</td><td colspan="2">True Image of the inclusion with circular shape(Case A)</td></tr>
<tr><td colspan="2"> 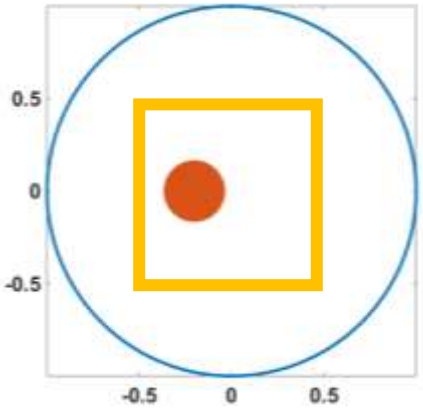
</td></tr>
<tr><td>CaseA(Tikhonov with 2% noise)</td><td>CaseA(TV with 2% noise)</td></tr>
<tr><td> 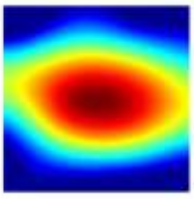 </td><td> 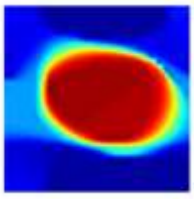 </td></tr>
<tr><td>Combined(Tikhonov with 2%noise)</td><td>Combined(TV with 2%noise)</td></tr>
</table>

			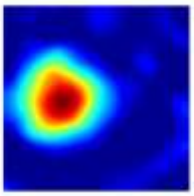	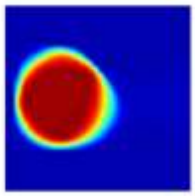

Table 6: Set5 Simulation with Single Inclusion of Radius 0.1 at Location (0.2, 0)

	Location	Size		
SET 5	(-0.2,0)	r =0.1	True Image of the inclusion with circular shape(Case A)	
			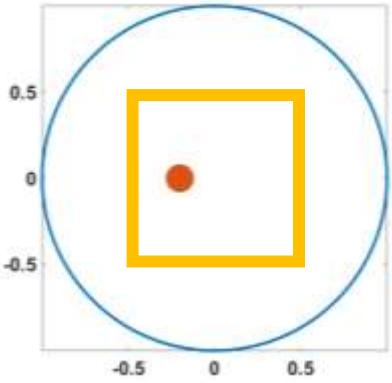	
			CaseA(Tikhonov with 2% noise)	CaseA(TVwith 2% noise)
			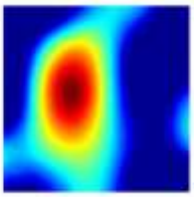	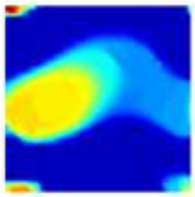
			Combined(Tikhonov with 2%noise)	Combined(TV with 2%noise)

			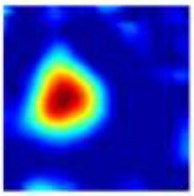	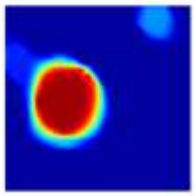

Table 7: Set6 Simulation with Single Inclusion of Radius 0.2 at Location (-0.3, 0)

	Location	Size		
SET 6	(-0.3,0)	r=0.2	True Image of the inclusion with circular shape(Case A)	
			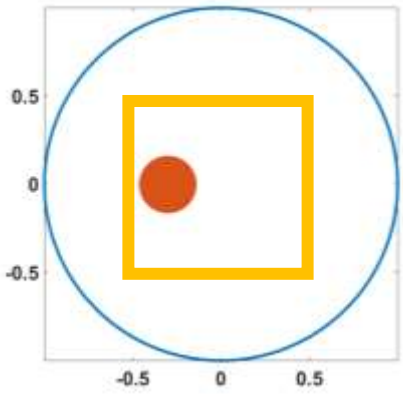	
			CaseA(Tikhonov with 2% noise)	CaseA(TV with 2% noise)
			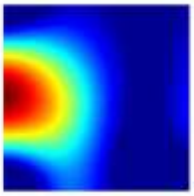	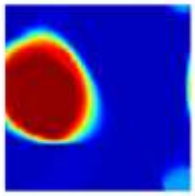
			Combined(Tikhonov with 2%noise)	Combined(TV with 2%noise)

			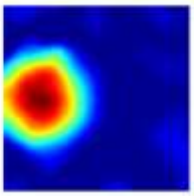	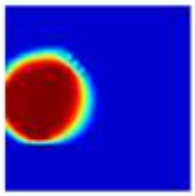

Table 8: Set7 Simulation with Single Inclusion of Radius 0.2 at Location (0.3, 0)

	Location	Size		
SET 7	(0.3,0)	r=0.2	True Image of the inclusion with circular shape(Case A)	
			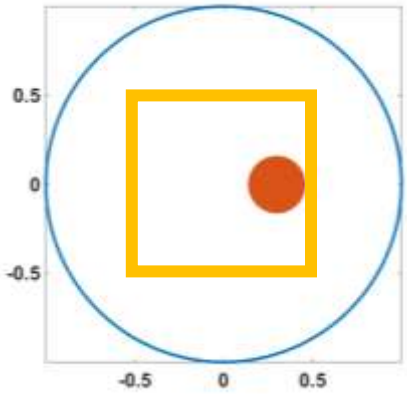	
			CaseA(Tikhonov with 2% noise)	CaseA(TV with 2% noise)
			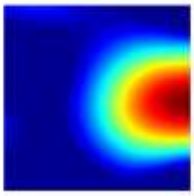	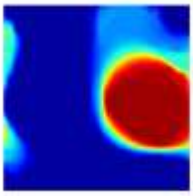
			Combined(Tikhonov with 2%noise)	Combined(TV with 2%noise)

			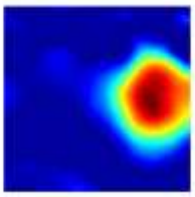	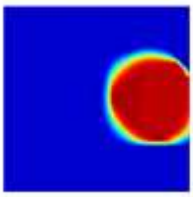

Table 9: Set8 Simulation with Single Inclusion of Radius 0.1 at Location (0, 0)

	Location	Size		
SET 8	（0,0）	r=0.1	True Image of the inclusion with circular shape(Case A)	
			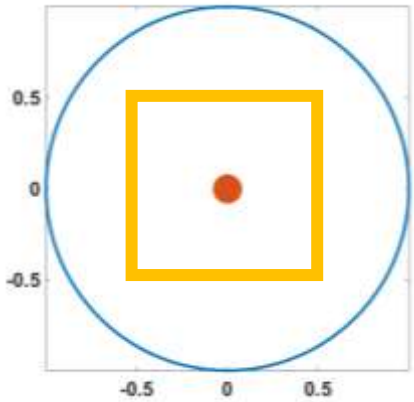	
			CaseA(Tikhonov with 2% noise)	CaseA(TV with 2% noise)
			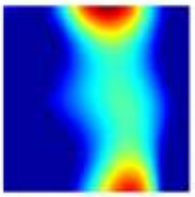	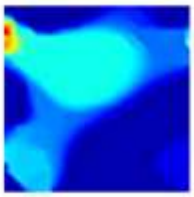
			Combined(Tikhonov with 2%noise)	Combined(TV with 2%noise)

			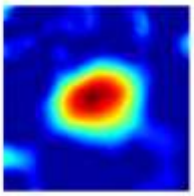	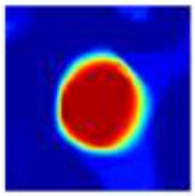

Table 10: Set9 Simulation with Single Inclusion of Radius 0.3 at Location (0, 0)

<table>
<tr><td></td><td>Location</td><td>Size</td><td colspan="2"></td></tr>
<tr><td rowspan="5">SET 9</td><td rowspan="5">(0,0)</td><td rowspan="5">r=0.3</td><td colspan="2">True Image of the inclusion with circular shape(Case A)</td></tr>
<tr><td colspan="2"> 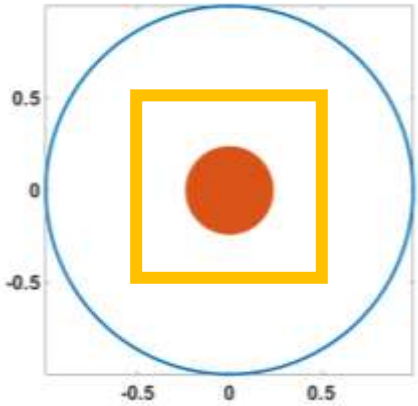
</td></tr>
<tr><td>CaseA(Tikhonov with 2% noise)</td><td>CaseA(TV with 2% noise)</td></tr>
<tr><td> 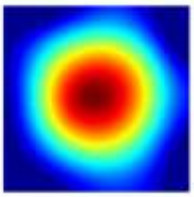 </td><td> 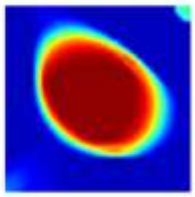 </td></tr>
<tr><td>Combined(Tikhonov with 2%noise)</td><td>Combined(TV with 2%noise)</td></tr>
</table>

			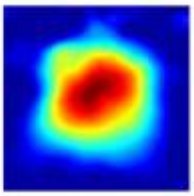	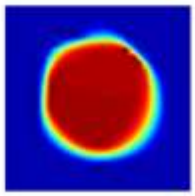

Sets 11-14 are simulations conducted with two inclusions. It is evident from the simulations that the Tikhonov method works better with multiple inclusions. Although Tikhonov method cannot demonstrate the clear separation of the two objects, it provides an image with the correct location, while TV fails in the case of smaller objects. Table 11 shows that in the case of two different sized inclusions, the conventional reconstruction did not show any separation of the two inclusion because the smaller inclusion was largely affected by the larger one. Regarding a combined case, although the Tikhonov method did not clearly show the smaller inclusion, it showed the trend of the separation.

Table 12,

Table 13 and

Table 14 show that by using the combined method, a clear separation is defined for both small and large items.

Table 13 also shows that when two inclusions are very close to each other, the combined method represents them better.

Table 11: Set10 Two Inclusions of Radius 0.2 and 0.1 at Corresponding Location (-0.2, 0) and (0.2, 0)

	location	size	

<table>
<tr><td rowspan="6">SET 10</td><td rowspan="6">p1(-0.2,0)

p2(0.2,0)</td><td rowspan="6">R(p1)=0.2;

R(p2)=0.1</td><td colspan="2">True Image of the inclusion with circular shape(Case A)</td></tr>
<tr><td colspan="2"> 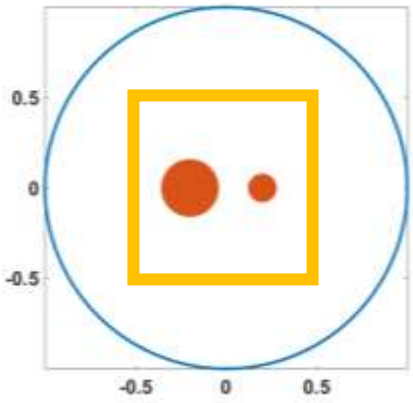
</td></tr>
<tr><td>CaseA(Tikhonov with 2% noise)</td><td>CaseA(TV with 2% noise)</td></tr>
<tr><td> 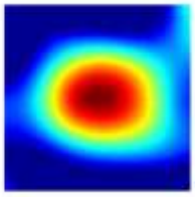 </td><td> 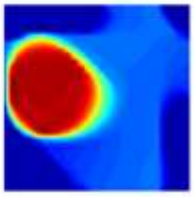 </td></tr>
<tr><td>Combined(Tikhonov with 2%noise)</td><td>Combined(TV with 2%noise)</td></tr>
<tr><td> 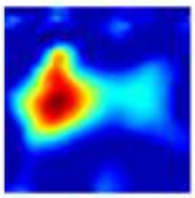 </td><td> 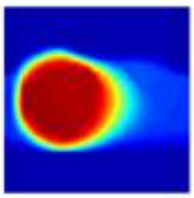 </td></tr>
</table>

Table 12: Set11 Two Inclusions of Radius 0.2 and 0.1 at Corresponding Location (-0.2, 0) and (0.2, 0)

	location	size	
SET 11	p1(-0.2,0)	R(p1)=0.1;	True Image of the inclusion with circular shape(Case A)

	p2(0.2,0)	R(p2)=0.1	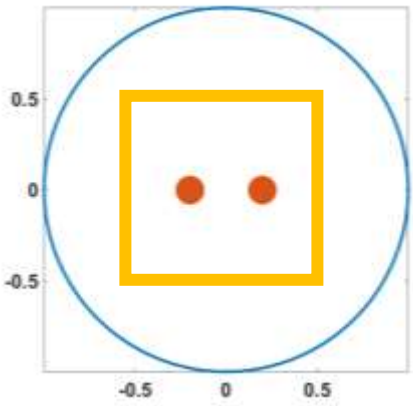
			CaseA(Tikhonov with 2% noise) / CaseA(TV with 2% noise)
			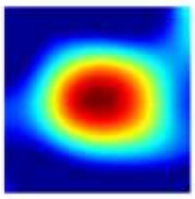 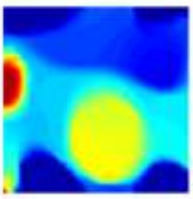
			Combined(Tikhonov with 2%noise) / Combined(TV with 2%noise)
			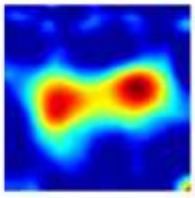 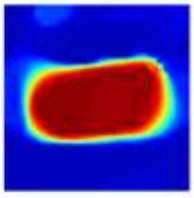

Table 13: Set12 Two Inclusions of Radius 0.2 and 0.2 at Corresponding Location (-0.2, 0) and (0.2, 0)

	location	size	
SET 12	p1(-0.2,0)	R(p1)=0.2;	True Image of the inclusion with circular shape(Case A)

<table>
<tr><td></td><td>p2(0.2,0)</td><td>R(p2)=0.2</td><td colspan="2"> 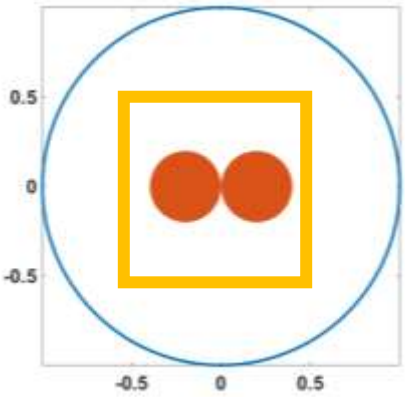
</td></tr>
<tr><td></td><td></td><td></td><td>CaseA(Tikhonov with 2% noise)</td><td>CaseA(TV with 2% noise)</td></tr>
<tr><td></td><td></td><td></td><td> 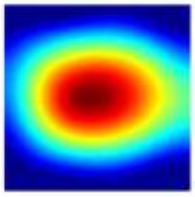 </td><td> 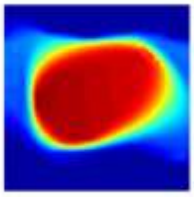 </td></tr>
<tr><td></td><td></td><td></td><td>Combined(Tikhonov with 2%noise)</td><td>Combined(TV with 2%noise)</td></tr>
<tr><td></td><td></td><td></td><td> 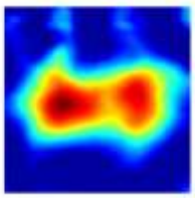 </td><td> 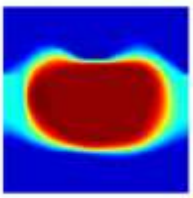 </td></tr>
</table>

Table 14: Set13 Two Inclusions of Radius 0.2 and 0.2 at corresponding Location (-0.3, 0) and (0.3, 0)

	location	size	
SET 13	p1(-0.3,0)	R(p1)=0.2;	True Image of the inclusion with circular shape(Case A)

<table>
<tr><td></td><td>p2(0.3,0)</td><td>R(p2)=0.2</td><td colspan="2"> 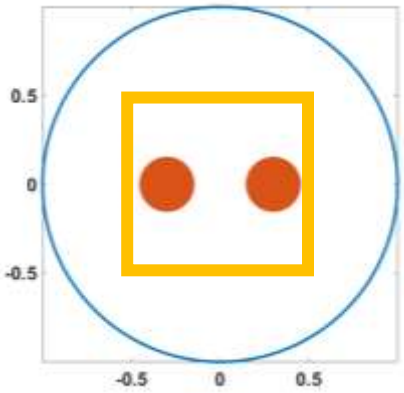
</td></tr>
<tr><td></td><td></td><td></td><td>CaseA(Tikhonov with 2% noise)</td><td>CaseA(TV with 2% noise)</td></tr>
<tr><td></td><td></td><td></td><td> 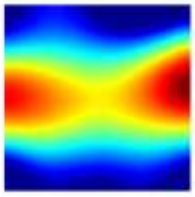 </td><td> 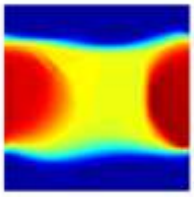 </td></tr>
<tr><td></td><td></td><td></td><td>Combined(Tikhonov with 2%noise)</td><td>Combined(TV with 2%noise)</td></tr>
<tr><td></td><td></td><td></td><td> 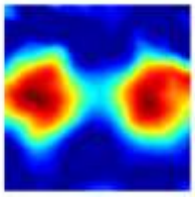 </td><td> 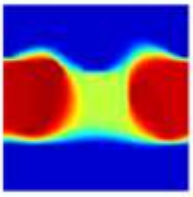 </td></tr>
</table>

4. Discussion

Breast Cancer is classified in different stages regarding to the tumour size, lymph node invasion and metastatic spread (the TNM system) (Taherian-Fard, Srihari, & Ragan, 2014). ‘T appended with a number (0–4) is used to describe the size and location of the tumour: T0—no evidence of tumour; T1—the invasive part of the tumour has size 20 mm and is carcinoma in situ, confined within the ducts or lobules of breast

tissue; T2—the invasive part of the tumour is 20–50 mm; T3—the invasive part >50 mm; and T4—the tumour has grown into the chest wall and skin with signs of inflammation.'The curative ratio and survival rate are much higher at early stages with smaller tumours.

Here 1D-plots of SET1 and SET8 are shown in Figure and Figure for two inclusions with different sizes in the centre. For a larger inclusion, total variation works better than the Tikhonov method, but for smaller objects both methods failed the single boundary measurement of case A. In both cases, the combined method could detect the inclusion. Particularly for a smaller object, the combined method provides a significant improvement in the results, especially in terms of increasing the detectability and the stability of detecting smaller objects. Therefore, applying the combined method can potentially be useful in breast cancer screening as early diagnosis is the key to the breast cancer treatments.

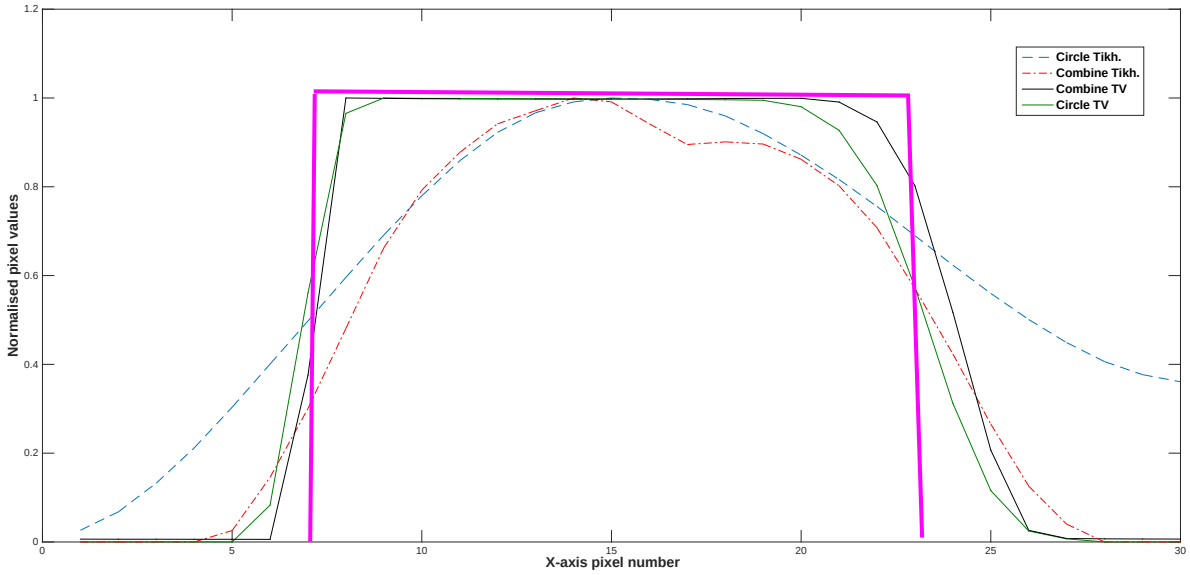

Figure 5 1-D Plot of an Inclusion of Size 0.2 in the Center（SET1). (The fuchsia line represents ideal results)

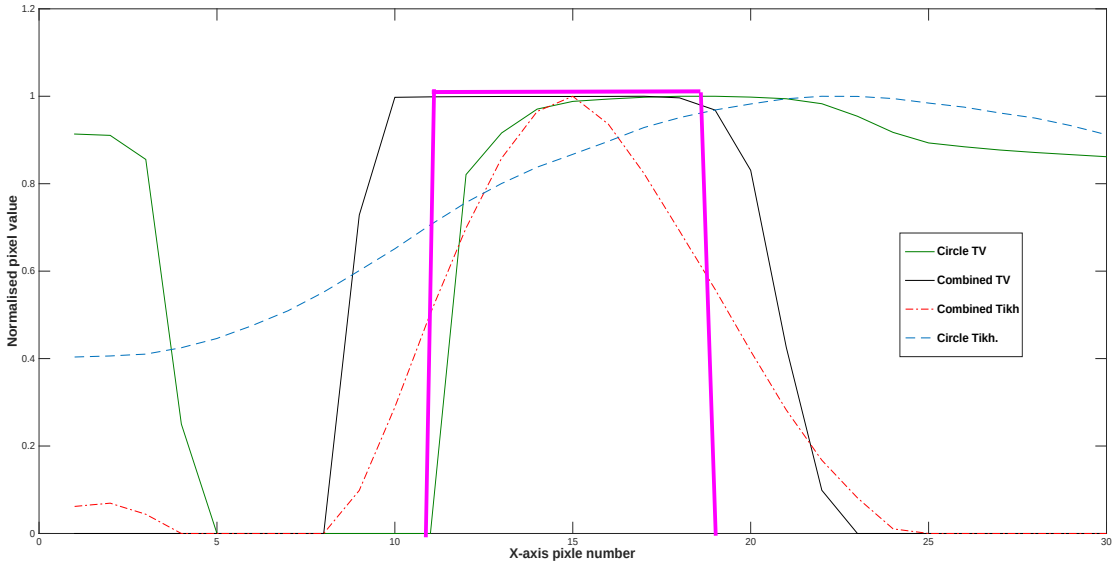

Figure 6 1-D Plot of an Inclusion of Size 0.1 in the Center (SET 8). (The fuchsia line represents ideal results)

Electrical conductivity varies not only for different body parts, organs, and types of tissues but also by the physiological state of the individual parts. Difference image is used instead of absolute imaging because of its ability to eliminate the background errors between each measurement by subtracting. Time-difference electrical impedance tomography (tdEIT) is widely used in EIT reconstructions. However, in order to achieve the result, a time dependent data measurement of the experimental objects is required. For certain applications such as tumour detection, it is almost impossible to acquire background data before the measurement with existing tumours. Therefore, frequency-difference EIT (fdEIT) is purposed to image frequency-dependant changes of a complex conductivity distribution within the imaged region (Seo, Lee, Kim, Zribi, & Woo, 2008). Studies (Surowiec, Stuchly, Barr, & Swarup, 1988) (Jossinet, 1996) (Jossinet & Schmitt, 1999) have shown a significant contrast between normal and pathological breast tissue in frequency response. The results shown here, therefore, could apply to fdEIT, because they measure two different frequencies in the same boundary position. Initial phantom design and test has been done and future work will follow in our continued study with biological samples and frequency difference measurements. Further investigation of combined modelling with experimental study is subject of our future studies.

5. Conclusions

EIT has been investigated as a non-invasive imaging technique for breast cancer for over two decades. Since EIT requires direct contact with the boundary, electrodes positioning errors and boundary movement have been considered as one of the sources of errors. Previous studies (Boyle, Adler, & Lionheart, 2012)

worked on shape recovery and correction to reduce the errors. However, unlike other parts of body such as the brain and the thorax, breast tissues are more elastic, and thus the deformation of the boundary shape is achievable. In this paper, a hypothesis of combining measurements with multiple shapes is discussed and validated with simulation. With the deformation of the boundary shape of the breast, the number of independent measurements has increased. It is shown in Figure 2 that more information data has been gathered as a result of combing multiple measurements. Models of different shapes have been developed to carry out the simulation. The choice of the shapes is arbitrary in this paper. To combine these different sets of information, a square of the region of interest has been selected with the inclusion inside. To maintain the consistency of the Jacobian method, the inclusion within the region remained unchanged after the deformation. For each set of simulation, 2% Gaussian noise (2% of the mean value of the measured voltage differences) has been added. Tikhonov regularization and TV are both used for the simulation. Simulation results indicated improvements in the detectability and the stability of detecting small objects. If the improvements suggested by simulation studies can be shown in experimental and in clinical data, these may become a very useful step in breast cancer screening as early diagnosis is key to breast cancer treatments. The experimental verification of the proposed method will follow in our continued study.

References

Boyle, A., Adler, A., & Lionheart, W. R. (2012, 12). Shape Deformation in Two-Dimensional Electrical Impedance Tomography. *IEEE Transactions on Medical Imaging*, pp. 2185-2193.

Goldsteom, T., & Osher, S. (2009). The split Bregman method for L1-regularized problems. *SIAM Journal on Imaging Sciences*, 323-343.

Jossinet, J. (1996). Variability of impedivity in normal and pathological breast tissue. *Med Biol Eng Computer*, 346-350.

Jossinet, J., & Schmitt, M. (1999). A review of parameters for the bioelectrical characterization of breast tissue. *Annals of the new york academy of sciences*, 30-41.

Lionheart, W., Polydorides, N., & Borsic, A. (2005). The Reconstruction Problem. In D. Holder (Ed.), *Electrical Impedance Tomography: Methods, History and Applications* (pp. 51-54). London: IOP Publising Ltd.

Lloyd, M., & Nash, A. (2001). 'Occult' breast cancer. *Ann R Coll Surg Engl*, pp. 420-424.

Mulcanhy, N. (2015, 10 16). *Screening Mammography Benifits and Harms in Spotlight Again*. Retrieved from Medscape: http://www.medscape.com/viewarticle/590535

Nagwa Dongola, M. (2015, 10 16). *Mammography in Breast Cancer*. Retrieved from MedScape: http://emedicine.medscape.com/article/346529-overview

Office for National Statistics. (2016, May 27). *Cancer Registration Statistics,England:2014 statistical bulletin.* Retrieved from Office for National Statistics: http://www.ons.gov.uk/peoplepopulationandcommunity/healthandsocialcare/conditionsanddiseases/bulletins/cancerregistrationstatisticsengland/2014#the-most-common-cancers-registered-were-breast-prostate-lung-and-colorectal-cancers

Oh, T. I., Wi, H., Kim, D. Y., Yoo, P. J., & Woo, E. J. (2011). Fully parallel multi-frequency EIT system with flexible electrode configuration：KHU Mark2. *Phys Meas*, 835-849.

Seo, J. K., Lee, J., Kim, S. W., Zribi, H., & Woo, E. J. (2008). Frequency difference electrical impedance tomography(fdEIT):algorithm development and feasibility study. *Physiol Meas*, 929-944.

SHA, L., WARD, E. R., & STORY, B. (2002). A Review of Dielectric Properties of Normal and Maligant Breast Tissue. *Proceedings IEEE SoutheastCon* (pp. 457-462). IEEE.

Surowiec, A. J., Stuchly, S. S., Barr, J. B., & Swarup, A. (1988). Dielectric properties of breast carcinoma and the surrounding tissues. *IEEE Trans BioMed Eng*, 257-263.

Taherian-Fard, A., Srihari, S., & Ragan, M. A. (2014, June 20). Breast Cancer classification:linking molecualar mechanisms to disease prognosis. *Briefings in BIOINFORMATICS*, pp. 461-474.

Tidswell, T., Gibson, A., Bayford, R. H., & Holder, D. S. (2000, June 30). Three-Dimensional Electrical Impedance Tomography of Human Brain Acticity . *NeuroImage*, pp. 283-294.

Vauhkonen, P. J., Vauhkonen, M., Savolainen, T., & Kaipio, J. P. (1999). Three-Dimensional Electrical Impedance Tomography Based on the Complete Electrode Model. *IEEE Transactions on Biomedical Engineering, 46*(9), 1150-1160.